

Terahertz epsilon-near-zero graded-index lens

Víctor Torres,^{1,2,*} Víctor Pacheco-Peña,¹ Pablo Rodríguez-Ulibarri,¹
Miguel Navarro-Cía,^{3,4,5} Miguel Beruete,¹ Mario Sorolla,¹ and Nader Engheta²

¹TERALAB (MmW – THz – IR & Plasmonics Laboratory), Universidad Pública de Navarra, Pamplona 31006, Spain

²Department of Electrical and Systems Engineering, University of Pennsylvania, Philadelphia 19104, USA

³Optical and Semiconductor Devices Group, Department of Electrical and Electronic Engineering, Imperial College London, London SW7 2BT, UK

⁴Centre for Plasmonics and Metamaterials, Imperial College London, London SW7 2AZ, UK

⁵Centre for Terahertz Science and Engineering, Imperial College London, London SW7 2AZ, UK

*victor.torres@unavarra.es

Abstract: An epsilon-near-zero graded-index converging lens with planar faces is proposed and analyzed. Each perfectly-electric conducting (PEC) waveguide comprising the lens operates slightly above its cut-off frequency and has the same length but different cross-sectional dimensions. This allows controlling individually the propagation constant and the normalized characteristic impedance of each waveguide for the desired phase front at the lens output while Fresnel reflection losses are minimized. A complete theoretical analysis based on the waveguide theory and Fermat's principle is provided. This is complemented with numerical simulation results of two-dimensional and three-dimensional lenses, made of PEC and aluminum, respectively, and working in the terahertz regime, which show good agreement with the analytical work.

©2013 Optical Society of America

OCIS codes: (080.3630) Lenses; (070.0070) Fourier optics and signal processing; (160.1245) Artificially engineered materials; (160.3918) Metamaterials.

References and links

1. L. Solymar and E. Shamonina, *Waves in Metamaterials* (Oxford, 2009).
2. N. Engheta and R. W. Ziolkowski, *Metamaterials: Physics and Engineering Explorations* (Wiley, 2006).
3. D. R. Smith, W. J. Padilla, D. C. Vier, S. C. Nemat-Nasser, and S. Schultz, "Composite medium with simultaneously negative permeability and permittivity," *Phys. Rev. Lett.* **84**(18), 4184–4187 (2000).
4. R. W. Ziolkowski, "Propagation in and scattering from a matched metamaterial having a zero index of refraction," *Phys. Rev. E Stat. Nonlin. Soft Matter Phys.* **70**(4), 046608 (2004).
5. M. G. Silveirinha and N. Engheta, "Tunneling of electromagnetic energy through subwavelength channels and bends using ϵ -near-zero materials," *Phys. Rev. Lett.* **97**(15), 157403 (2006).
6. A. Alù, M. G. Silveirinha, A. Salandrino, and N. Engheta, "Epsilon-near-zero metamaterials and electromagnetic sources: tailoring the radiation phase pattern," *Phys. Rev. B* **75**(15), 155410 (2007).
7. C. Bohren and D. Huffmann, *Absorption and Scattering of Light by Small Particles* (Wiley, 1983).
8. J. D. Jackson, *Classical Electrodynamics* (Wiley, 1999).
9. J. Gómez Rivas, C. Janke, P. Bolivar, and H. Kurz, "Transmission of THz radiation through InSb gratings of subwavelength apertures," *Opt. Express* **13**(3), 847–859 (2005).
10. P. B. Johnson and R. W. Christy, "Optical constants of the noble metals," *Phys. Rev. B* **6**(12), 4370–4379 (1972).
11. A. Alù, M. G. Silveirinha, and N. Engheta, "Transmission-line analysis of ϵ -near-zero-filled narrow channels," *Phys. Rev. E Stat. Nonlin. Soft Matter Phys.* **78**(1), 016604 (2008).
12. H. Shi, C. Wang, C. Du, X. Luo, X. Dong, and H. Gao, "Beam manipulating by metallic nano-slits with variant widths," *Opt. Express* **13**(18), 6815–6820 (2005).
13. L. Verslegers, P. B. Catrysse, Z. Yu, J. S. White, E. S. Barnard, M. L. Brongersma, and S. Fan, "Planar lenses Based on Nanoscale Slit Arrays in a metallic film," *Nano Lett.* **9**(1), 235–238 (2009).
14. Z. Sun and H. K. Kim, "Refractive transmission of light and beam shaping with metallic nano-optic lenses," *Appl. Phys. Lett.* **85**(4), 642–644 (2004).
15. C. Ma, M. Escobar, and Z. Liu, "Extraordinary light focusing and Fourier transform properties of gradient-index metalenses," *Phys. Rev. B* **84**(19), 195142 (2011).
16. C. Ma and Z. Liu, "A super resolution metalens with phase compensation mechanism," *Appl. Phys. Lett.* **96**(18), 183103 (2010).
17. L. Verslegers, P. B. Catrysse, Z. Yu, and S. Fan, "Deep-subwavelength focusing and steering of light in an aperiodic metallic waveguide array," *Phys. Rev. Lett.* **103**(3), 033902 (2009).

18. S. Ishii, A. V. Kildishev, V. M. Shalaev, K. P. Chen, and V. P. Drachev, "Metal nanoslit lenses with polarization-selective design," *Opt. Lett.* **36**(4), 451–453 (2011).
19. S. Ishii, A. V. Kildishev, V. M. Shalaev, and V. P. Drachev, "Controlling the wave focal structure of metallic nanoslit lenses with liquid crystals," *Laser Phys. Lett.* **8**(11), 828–832 (2011).
20. S. Ishii, V. M. Shalaev, and A. V. Kildishev, "Holey-metal lenses: sieving single modes with proper phases," *Nano Lett.* **13**(1), 159–163 (2013).
21. D. M. Pozar, *Microwave Engineering* (Wiley, 2005).
22. B. Edwards, A. Alù, M. E. Young, M. Silveirinha, and N. Engheta, "Experimental verification of epsilon-near-zero metamaterial coupling and energy squeezing using a microwave waveguide," *Phys. Rev. Lett.* **100**(3), 033903 (2008).
23. M. G. Silveirinha and N. Engheta, "Theory of supercoupling, squeezing wave energy, and field confinement in narrow channels and tight bends using ϵ near-zero metamaterials," *Phys. Rev. B* **76**(24), 245109 (2007).
24. R. E. Collin, *Foundations for Microwave Engineering* (Wiley, 2000).
25. M. Beruete, I. Campillo, M. Navarro-Cia, F. Falcone, and M. Sorolla Ayza, "Molding left- or right-handed metamaterials by stacked cutoff metallic hole arrays," *IEEE Trans. Antenn. Propag.* **55**(6), 1514–1521 (2007).
26. M. Navarro-Cia, M. Beruete, M. Sorolla, and N. Engheta, "Lensing system and Fourier transformation using epsilon-near-zero metamaterials," *Phys. Rev. B* **86**(16), 165130 (2012).
27. D. Filipovic, S. Gearhart, and G. Rebeiz, "Double-slot antennas on extended hemispherical and elliptical silicon dielectric lenses," *IEEE T. Microw. Theory* **41**(10), 1738–1749 (1993).
28. N. Llombart, G. Chattopadhyay, A. Skalare, and I. Mehdi, "Novel terahertz antenna based on a silicon lens fed by a leaky wave enhanced waveguide," *IEEE Trans. Antenn. Propag.* **59**(6), 2160–2168 (2011).
29. Microtech Instruments Inc, <http://mtinstruments.com>
30. Thorlabs Inc, <http://www.thorlabs.com>
31. J. W. Goodman, *Introduction to Fourier Optics* (Roberts & Company Publishers, 2004).
32. W. Kock, "Metal-lens antennas," *Proceedings of the IRE* **34**(11), 828–836 (1946).
33. J. Ruze, "Wide-angle metal-plate optics," *Proceedings of the IRE* **38**(1), 853–855 (1950).
34. M. Navarro-Cia, M. Beruete, I. Campillo, and M. Sorolla Ayza, "Beamforming by left-handed extraordinary transmission metamaterial bi- and plano-concave lens at millimeter-waves," *IEEE Trans. Antenn. Propag.* **59**(6), 2141–2151 (2011).
35. H. D. Hristov, *Fresnel Zones in Wireless Links, Zone Plate Lenses and Antennas* (Artech House, 2000).
36. M. Navarro-Cia, M. Beruete, I. Campillo, and M. Sorolla, "Enhanced lens by ϵ and μ near-zero metamaterial boosted by extraordinary optical transmission," *Phys. Rev. B* **83**(11), 115112 (2011).

1. Introduction

The challenge of engineering and controlling the electromagnetic properties of materials is on the forefront of basic materials science and engineering. Electromagnetic metamaterials have followed this trail, focusing on the control of electromagnetic fields [1,2]. In order to surpass the limits available in natural materials, metamaterials with unconventional values of permittivity (ϵ) or permeability (μ) have been extensively studied during the last decades. The realization of a double negative medium [3] was one of the most relevant advances in material science. Afterwards, metamaterials with an effective index of refraction near zero ($n \rightarrow 0$) [4] and, more recently, metamaterials with low permittivity, so called ϵ -near-zero (ENZ) [5,6], have become subject of extensive investigation.

Extreme values of the permittivity (i.e. near-zero or very large) can be found in dispersive natural materials. In these materials, permittivity is dispersive due to internal molecular resonances where their frequency response can be approximated by Drude-Lorentz models [7,8]. By definition, at the plasma frequency of a Drude medium the real part of the permittivity effectively goes to zero and at the resonance of a Lorentzian medium, the permittivity may become very large. However, this behavior is usually found at mid infrared frequencies for polar dielectrics and lightly-doped semiconductors [9], and in the visible and ultraviolet for noble metals [10]. Therefore engineered materials, i.e. metamaterials, are needed to obtain such electromagnetic singularities at the lower frequency bands such as microwaves or terahertz waves.

A typical procedure to obtain ENZ metamaterials is to employ an arrangement of perfectly-electric conducting (PEC) metallic waveguides working near their cut-off frequencies [11]. By tuning the dimensions of the waveguides it is possible to have good impedance matching at the frequency where the effective permittivity tends to zero. In this work, we theoretically study and numerically confirm the realization of a graded index ENZ lens based on these waveguide configurations [11]. The dimensions of each waveguide is designed independently in order to have the desired propagation constant and thus phase

delay inside each waveguide for achieving a flat convergent lens while each waveguide remains approximately impedance matched to free-space. With this approach Fresnel reflection is significantly reduced. Several realizations of planar graded-index lenses composed of slit arrays with non-uniform width have been proposed and demonstrated in the past by other groups [12–20]. Although most of these lenses manipulate the phase delay inside each slit in an analogous fashion as we do here, they do so using the modes in waveguides with plasmonic walls, and they do not address the issue of the mismatch between the guided mode and the incident illumination. Some of them are also suitable for focusing in one plane, not two. As we will discuss below, here we use one dimension of the cross section of the hollow waveguide made of PEC walls to adapt the phase delay and the other one to effectively match our lens to the incoming plane-wave propagating in free-space.

2. Analytical formulation

Attending to the classical waveguide theory, we know that hollow rectangular waveguides made of PEC walls can propagate TM and TE modes above the cut-off frequency, whereas below the cut-off frequency the modes are evanescent [21]. The mode with the lowest cut-off frequency is called the dominant mode, and depending on the dimensions of the waveguide cross section and the orientation of the fields, this mode is unique. For a rectangular waveguide of dimensions h_x and h_y with $h_y > h_x$ and E-field oriented in the x -direction, the fundamental mode is the TE_{01} whose cut-off frequency is $f_c^{TE_{01}} = c/2h_y$, where c is the velocity of light in free space and it is assumed that the guide is filled with free space (or air). The propagation constant of this mode can be written as

$$\beta = k_0 \sqrt{1 - \left(\frac{f_c^{TE_{01}}}{f} \right)^2} = k_0 \sqrt{1 - \left(\frac{\pi}{k_0 h_y} \right)^2}, \quad (1)$$

where $k_0 = 2\pi f \sqrt{\mu_0 \epsilon_0}$ is the wave number in free space. It was theoretically demonstrated in [11] and experimentally verified in [22] that working slightly above the cut-off frequency, a microwave metallic waveguide may behave as an ENZ metamaterial. Near the cut-off frequency the propagation constant is very small, as shown by Eq. (1). Thus the relative effective permittivity of the waveguide ϵ_{w_eff} is very close to zero, since:

$$\epsilon_{w_eff} = 1 - \left(\frac{f_c^{TE_{01}}}{f} \right)^2 = 1 - \left(\frac{\pi}{k_0 h_y} \right)^2, \quad (2)$$

where it has been assumed that the effective permeability of the waveguide is μ_0 . From here we can obtain an expression for the accumulated phase variation within the ENZ in terms of the waveguide dimensions:

$$\Delta\theta_w = \beta L = \left(k_0 \sqrt{1 - \left(\frac{\pi}{k_0 h_y} \right)^2} \right) L, \quad (3)$$

where L is the waveguide length. Due to the low propagation constant of the guided mode (β), a small phase variation occurs even over a physically long distance. Moreover, with slight variations in the h_y dimension, we are able to control with high accuracy the propagation constant and consequently the phase of the mode. Thus, we have the basic ingredients for a graded-index lens, where the phase variation of each waveguide is carefully tuned to transform an incident plane wave into a spherical wave. Figure 1(a) illustrates this idea.

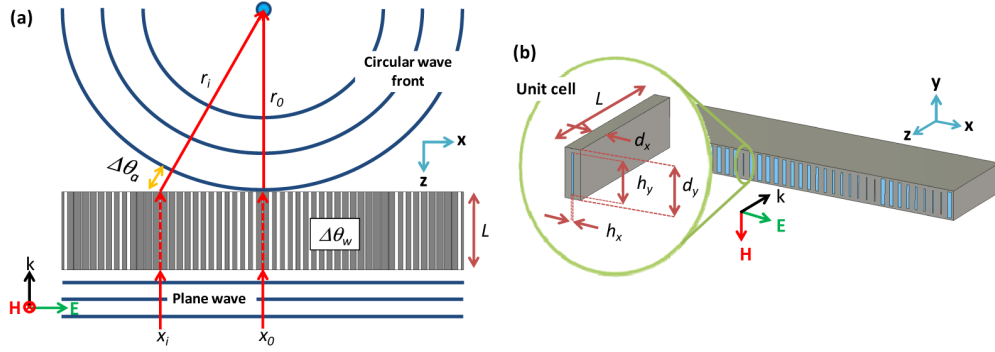


Fig. 1. (a) Schematic of a plane wave with TM-polarization impinging on an arrangement of metallic waveguides of constant length L . For each waveguide, width (h_x) and height (h_y) are determined in order to achieve the required circular wave front with focal length r_0 . The values $\Delta\theta_w$ and $\Delta\theta_a$ are the phase delay inside the waveguide and the phase delay in the air, respectively. (b) Perspective view and unit cell detail of dimensions d_x and d_y .

For the central waveguide, choosing the height of the waveguide to work at $f = f_c$, leads to the effective permittivity is near zero, $\epsilon_{w_eff} \approx 0$. Therefore, theoretically, the wave propagates with no phase delay because the phase velocity is effectively infinite. Then, in order to obtain the desired phase at the output of each of the remaining channels, each waveguide should introduce a phase variation equal to

$$\Delta\theta_w(x_i) = 2\pi i - \Delta\theta_a(x_i) - \Delta\theta_w(x_i = 0) = 2\pi i - k_0(r_i - r_0) - \Delta\theta_w(x_i = 0), \quad (4)$$

where i is an integer number $i = 1, 2, \dots$; $\Delta\theta_a(x_i)$ is the phase delay in the air due to the difference in distance from the exit of each waveguide to the focus, with respect to the central waveguide ($r_i - r_0$), and $x_i = i \cdot d_x$ represents the x -coordinate of the center of each aperture. It is worth mentioning that $\epsilon_{w_eff} = 0$ is an ideal condition that in practice may never be achieved, partly because of absorption and partly due to the imperfection in the waveguide geometry. Also, note that this condition implies an unphysical infinite phase velocity. In practice, the frequency of operation will be close to - but not exactly at - the cut-off frequency, so the phase velocity will be very large but finite and, therefore, there will be a certain phase delay. This small phase delay at the central waveguide is taken into account in Eq. (4) by $\Delta\theta_w(x_i = 0)$. Finally, calculating all $\Delta\theta_w(x_i)$ we immediately obtain from Eq. (3) the height values of each aperture:

$$h_y(x_i) = \frac{\pi}{\sqrt{k_0^2 - \left(\frac{\Delta\theta_w(x_i)}{L}\right)^2}}. \quad (5)$$

At first glance, it might seem that the structure is completely mismatched to the free-space because of the apparent impedance contrast between air and the ENZ waveguides. However, the wave is able to tunnel through the structure coupling most of the energy, if at least one of the physical dimensions of the channel is electrically small, phenomenon that is known as supercoupling and energy squeezing, described in [5,23]. The ideal value for h_x can be obtained by analyzing the structure from a transmission line perspective [24] and matching the normalized characteristic line impedance of free space η_{air} and the waveguide η_w . Reducing the problem to the single unit cell detailed in the Fig. 1(b), η_{air} is defined in the air volume surrounding an artificial waveguide of dimensions d_x and d_y with electric and magnetic walls in x -direction and y -direction, respectively [25]; and η_w in the narrow channel of the ENZ waveguide of dimensions h_x and h_y . Thus, matching the impedances, we obtain:

$$\frac{d_x}{d_y} \sqrt{\frac{\mu_0}{\epsilon_0}} = \eta_{air} = \eta_w = \frac{h_x(x_i)}{h_y(x_i)} \sqrt{\frac{\mu_0}{\epsilon_0 \epsilon_{w_eff}}}. \quad (6)$$

Thereby, the width for each aperture needs to be

$$h_x(x_i) = \frac{\Delta\theta_w(x_i) d_x}{k_0 \cdot L d_y} h_y(x_i). \quad (7)$$

3. Two-dimensional lens

To begin with, let us analyze the ENZ waveguide array lens shown in Fig. 1(b) where the structure is considered infinite in the y -direction and is excited by an incident plane wave that propagates in the z direction and whose electric field vector is polarized along the x axis. For a design frequency f_0 equal to 1 THz ($\lambda_0 = 300 \mu\text{m}$), the thickness of the lens is assumed to be $L = 2\lambda_0$, the total width in the x -direction is equal to $10.2\lambda_0$ and the dimensions of the unit cell are $d_x = 60 \mu\text{m}$ and $d_y = 180 \mu\text{m}$. The dimensions of the narrow channels have been chosen to have the focus at $r_0 = 1.5 \text{ mm} = 5\lambda_0$ from the exit face. The material of the lens is assumed to be PEC and the boundary conditions have been fixed as open (perfectly matched layer) in the x -direction and magnetic walls in the upper and lower faces in order to make the structure infinitely periodic in the y -direction. For the numerical simulation the structure is meshed with accuracy equal to $\lambda_0/20$. For all the numerical results, we have used the finite-integration-technique software CST Microwave StudioTM.

A set of 51 waveguides is then designed with specific heights and widths determined from Eqs. (5) and (7). Figure 2(a) shows the design values for both dimensions of each of the 51 waveguides together with their corresponding phase variation, identified by the position in the x -direction. The abrupt changes in the dimensions of adjacent waveguides correspond to phase changes equal to 2π . Note in the figure that the values for $\Delta\theta_w$ have been calculated taking into account the fact that we really work at a frequency slightly above 1 THz, exactly at 1.0035 THz. The relative effective permittivity ϵ_{w_eff} of all waveguides retrieved from the numerical results is compared with the theoretical values in Fig. 2(b). We achieve good agreement between the simulated values and those calculated with the analytical formulation. Moreover, it is clearly seen that all waveguides are working around the ENZ region (i.e., low-epsilon region), obtaining the value closest to zero for the central waveguide, as it has been initially designed.

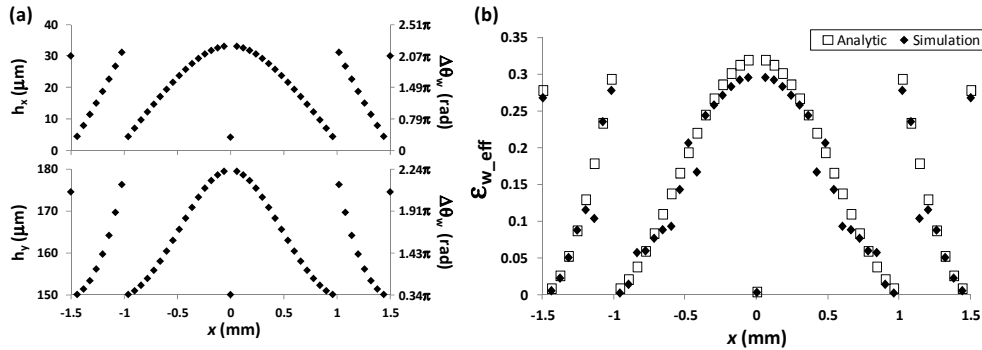


Fig. 2. (a) Dimensions of the waveguide width h_x , and height h_y , and phase variation $\Delta\theta_w$ of each waveguide for a 2D graded-index lens of total width 3.06 mm and focal length 1.5 mm. (b) Comparison between the relative effective permittivity of each ENZ waveguide obtained with simulation (open square) and analytical formulation (solid rhombus).

In Fig. 3(a), the numerically-computed magnetic field distribution along the xz -plane is shown. It can be observed that the planar phase front at the input is converted into a

cylindrical phase front at the exit of the lens. It is also evident from the figure the slight differences in the phase of the magnetic field inside each waveguide. Figure 3(b) shows the magnitude of the y -component of the magnetic field (H_y) and the x -component of the electric field (E_x) along z axis for the central waveguide. A focus is clearly observed for both fields, less evident in the E-field because it is hidden due to an enhancement of the electric field inside the lens. This enhancement of the E-field in the waveguides is not the same in all waveguides because the E_x magnitude is higher when the effective permittivity is closer to zero [5]. The same fields are represented along x at the focal plane in Fig. 3(c) showing the focus and a *sinc*-like spatial distribution for H_y and E_x , demonstrating that the epsilon-near-zero graded-index structure behaves indeed as a lens acting as a Fourier transform operator [26]. It is also worth noting that a standing wave appears at the lens input, which is caused by some reflections coming from the finite size in the x -direction. Therefore, edge effects are unavoidable and the value for the free space characteristic line impedance deviates slightly from the theoretical value obtained for an infinitely replicated single waveguide. The

approximate reflection coefficient $|\Gamma| = 0.3$ is obtained using the expression $\frac{A_{\max}}{A_{\min}} = \frac{1+|\Gamma|}{1-|\Gamma|}$,

with A_{\max} and A_{\min} as the maximum and minimum values of the field amplitude [21]. The impedance matching is quite good compared with typical dielectric lenses at terahertz frequencies [27,28], generally made of silicon whose relative permittivity (ϵ_r) is 11.9, leading to a reflection coefficient of 0.55. It is also possible to find commercial dielectric lenses for terahertz applications [29,30] made of Teflon ($\epsilon_r = 1.9$) or Tsurupica ($\epsilon_r = 2.31$) whose reflection coefficient would be lower than 0.3, assuming lossless dielectrics. However, lenses made from the latter dielectrics have thicknesses around $10\lambda_0$, five times greater than our design.

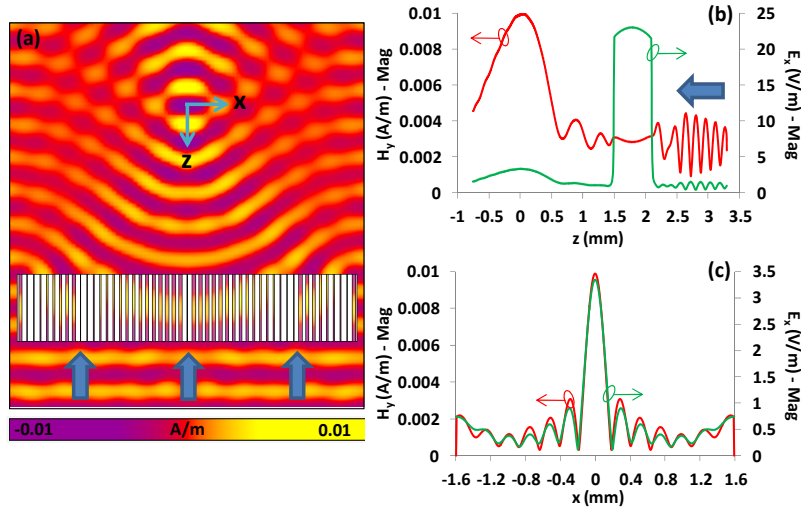


Fig. 3. (a) Top view (xz -plane) of the magnetic field distribution H_y on a system composed of a flat metallic lens made of arrangement of ENZ waveguides illuminated by a normally incident plane wave. (b) Magnetic field distribution H_y and electric field distribution E_x along the optical axis, z -direction; and (c) along the x -direction at the focal length.

The main features obtained for our lens are the enhancement factor (i.e. focus to incident intensity ratio) of 12.84, a depth of focus in the optical axis (z -direction) equal to $861.37 \mu\text{m} = 2.87\lambda_0$ and a full-width at half-maximum (FWHM) at the focal plane (x -direction) of $174.86 \mu\text{m} = 0.58\lambda_0$. It must be highlighted that with this completely flat graded-index ENZ lens, a reduction of 36.51% of the total volume of the lens is achieved with respect to an ENZ waveguide lens with a convex profile and same dimensions [26]. Notice that in this

comparison, the volume of the convex ENZ lens is computed by considering a rectangular cuboid with length equals to the length of the lateral waveguides

Table 1 shows a comparison of several designs with different sizes of the lens aperture, in order to evaluate the penalty in the performance of the lens when its aperture is reduced. As the total width is shortened, the enhancement factor is lowered because the number of waveguides that collects the impinging energy is reduced. Also, the greater values of depth of focus and FWHM show that the energy concentration is less effective. Attending to the focal length, the numerically-computed focus is just slightly shifted compared to the design. This is a direct consequence of working out of the ideal condition of effective permittivity of the central waveguide equal to zero. The number of apertures is also relevant for this parameter, as can be deduced from Table 1, since if there are not enough waveguides the phase front is no longer circular. Moreover, the diffraction caused by edge effects are more notable and further affect the focus. Under our design conditions, we have found the minimum of the total width with acceptable performance to be around $6\lambda_0$.

Table 1. Feature summary for a two-dimensional lens with different total widths

Number of Apertures (Width)	Focal Length (μm)	Enhancement Factor	Depth of Focus (μm)	FWHM (μm)
51 ($10.2\lambda_0$)	1475.31	12.84	861.37	174.86
41 ($8.2\lambda_0$)	1337.13	9.59	997.19	189.10
31 ($6.2\lambda_0$)	1337.20	7.24	1432.80	216.39

The behaviour of the lens under an obliquely incident plane wave illumination has also been analyzed. Figure 4 shows the cross section of the power along the focus plane when the angle of incidence is varied from 0 to 20 degrees. The focus shifts as expected according to Fourier analysis [26,31]. A reduction of the transmitted power is noticeable as the angle of incidence increases. For instance, the enhancement factor falls from 12.84 to 8.74 for 20 degrees angle of incidence. The numerical aperture calculated as $n \cdot \sin\theta$ where n is the index of refraction of the medium surrounding the lens, air in this case; and θ the half-angle of the maximum cone of incident wave that can enter or exit the lens, is equal to 0.472. The angle of the maximum cone of incidence is calculated as the angle for which the transmitted power at the focus is half the transmitted power at the focus under normal incident.

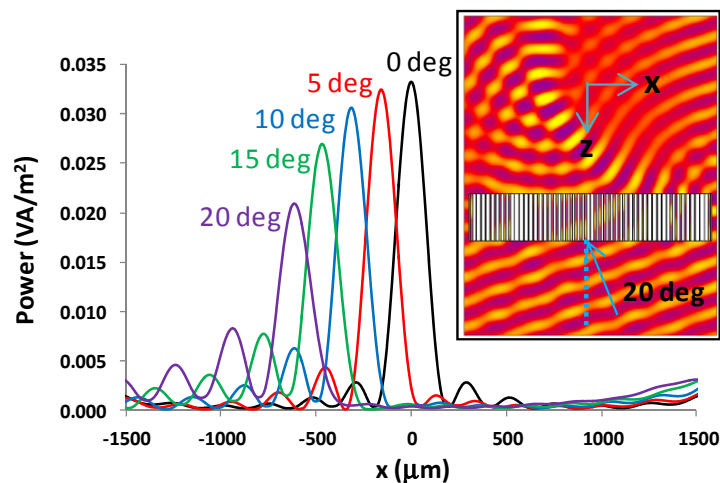


Fig. 4. Cross section of the power along x -direction at the focal plane when the input signal is an obliquely incident plane wave. It is represented from 0 to 20 degrees of angle of incidence in steps of 5 degrees. (inset) Top view (xz -plane) of the magnetic field distribution H_y along the focal plane for an input wave with an angle of incidence of 20 degrees.

Finally, Table 2 shows the behaviour of the lens for different operation frequencies in order to evaluate the chromatic dispersion/aberration of the lens. We observe that the focus moves further away as the frequency increases. This follows from Eq. (4). As the frequency increases, so does ϵ_{w_eff} , and thus, also the accumulated phase variations $\Delta\theta_w(x_i)$ and $\Delta\theta_w(x_i=0)$. Therefore, $(r_i - r_0)$ is enforced to be reduced, which happens when the focal length increases. The table also shows a general degradation of the performance of the lens compared to the optimal frequency 1.0035 THz (highlighted in bold in Table 2). This degradation is more severe for frequencies below the optimal frequency because the waveguides with lower values of h_y start to operate at cut-off. The bandwidth of operation, estimated as a -3 dB from the optimum enhancement factor, is 0.27 THz, corresponding to a fractional bandwidth of 26.9%. Moreover, the reflection coefficient increases as the frequency of operation deviates from the optimal frequency: we obtain $|\Gamma| = 0.48$ at 0.98 THz and $|\Gamma| = 0.65$ at 1.2 THz. Therefore, this lens works in a narrow band, which is limited by the frequency dispersion of the effective permittivity and the impedance matching.

Table 2. Feature Summary for a Two-dimensional Lens at Different Operation Frequencies

Operation Frequency (THz)	Focal Length (μm)	Enhancement Factor	Depth of Focus (μm)	FWHM (μm)
0.98	1311.90	6.16	1356.61	209.43
0.99	1436.82	8.20	943.77	183.21
1.0035	1475.31	12.84	861.37	174.86
1.10	1825.33	10.37	907.19	229.05
1.20	1937.90	7.64	963.35	554.76

4. Three-dimensional lens

Unlike some of the graded-index lenses based on slit arrays [12–20], the ENZ lens proposed here has the potential to achieve spherical phase fronts, i.e., convergence in two orthogonal planes. This is investigated next with the ENZ lens shown in Fig. 5(a). The design frequency is again $f_0 = 1$ THz so the dimensions of the unit cell are the same: $d_x = 60 \mu\text{m}$ and $d_y = 180 \mu\text{m}$. The total dimensions of the full structure are $L_x = L_y = 10.2\lambda_0 = 3.06$ mm and the thickness $L_z = 600 \mu\text{m}$. Moreover, in order to take into account metal losses, the structure is made of aluminium, with conductivity equal to 3.56×10^7 S/m. Figure 5(b) depicts the simulation results for the power distribution in the xz and yz -planes when the lens is excited with a plane wave with TM polarization, i.e. electric field polarized along x . It can be seen in both planes that the energy is focused demonstrating the performance of the lens. The enhancement factor is 62.3, and the focal length and depth of focus are equal to $1312.50 \mu\text{m} = 4.38\lambda_0$ and $614.04 \mu\text{m} = 2.05\lambda_0$ respectively. The cross section of the power along the focal plane in the x -direction and y -direction is shown in the inset of the Fig. 5(b). The FWHM is $184.04 \mu\text{m}$, resulting in a resolution of $1.23\lambda_0/2$, very close to half wavelength. Along the y -direction, the FWHM obtained is $190.60 \mu\text{m}$ equal to $1.27\lambda_0/2$. It is important to note that this design has been done to get the focus at $5\lambda_0$. It is worth mentioning that the flexibility of tailoring the phase difference between waveguides allows us to modify the focal length and/or to get different phase fronts at the output such as plane waves radiating in other directions or convex phase patterns, by just properly changing the dimensions of the individual waveguide cross section. Finally, the simulation results for the extinction ratio between copolar and crosspolar polarization at the focal distance is 51.32 dB allowing us to use this lens as a polarization analyzer as well.

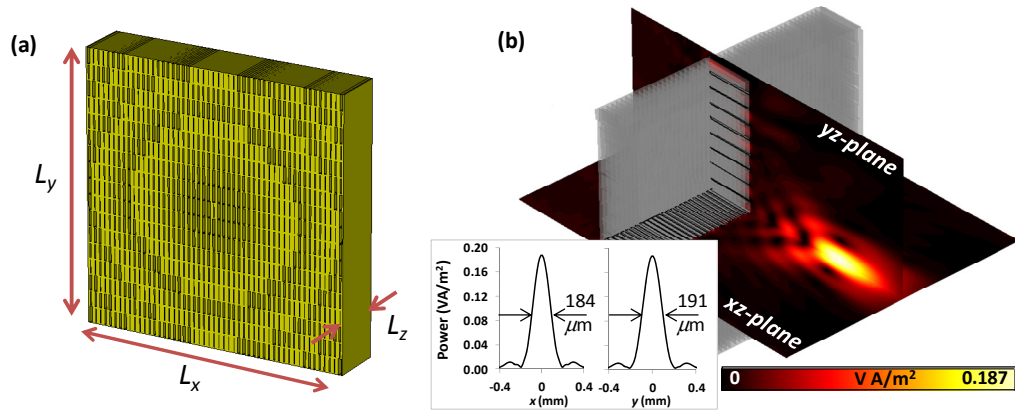


Fig. 5. (a) Sketch of the proposed 3D planar graded index lens, made of arrangement of ENZ waveguides, of total dimensions L_x and L_y and thickness L_z . (b) Power distribution along the xz - and yz -planes, and (inset) along the x -direction and y -direction when the structure is excited with a plane wave

A plane wave excitation is, in general, an ideal case that cannot be performed in most of the real experimental setups. For that reason and in order to emulate a realistic incident wave, the plane wave is replaced by a Gaussian beam [31]. The minimum beam radius is equal to $1496.95 \mu\text{m}$ and the excitation is defined to have the beam focus (that is, where the minimum beam radius is located) at 1.5 mm far from the lens face. This new system, Gaussian beam and lens, may emulate in a reliable way a real system composed by a horn antenna working at 1 THz that illuminates the lens. Figures 6(a) and 6(b) show the magnetic field distribution H_y for xz and yz -planes, respectively. The focus is clearly observed in both planes but more interesting is that the intensity of the field on the edges is lower than in the middle of the structure thanks to the Gaussian beam excitation, and thus spurious diffraction effects are reduced. This can be observed in further detail in Figs. 6(c) and 6(d), where the power distribution is shown on the xz - and yz -plane. With this new excitation the enhancement factor (now calculated with respect to the beam maximum value) is 24.3 . The obtained value of depth of focus is $700.41 \mu\text{m} = 2.33\lambda_0/2$ and the values of FWHM along x and y -direction are $210.8 \mu\text{m} = 1.41\lambda_0/2$ and $218.4 \mu\text{m} = 1.46\lambda_0/2$, respectively. Note that the performance of the focus is slightly worse than that of the plane wave excitation, as expected, since the contribution of the external waveguides is less effective.

The design of this lens may resemble classical metallic lenses such as constrained lenses [32–34] or Fresnel zone plates [35]. However, there are major differences arisen from their underlying physics. While classical lenses are based on an arrangement of waveguides working with fundamental modes well above their cut-off frequencies, the ENZ lenses use waveguides near cut-off. From an effective constitutive parameters point of view both lenses exhibit a permeability equal to one but the permittivity for constrained lenses is $0 < \epsilon < 1$ and for ENZ ones is obviously $\epsilon \rightarrow 0^+$. Consequently, attending to Fermat's principle [1], classical lenses always have ellipsoidal profiles and ENZ lenses cylindrical profiles if the graded-index techniques are not used. Furthermore, constrained lenses tend to display undesired grating lobes given the large in-plane periodicities, whereas the lens analyzed here prevents them in both planes, due to the subwavelength periodicity along the direction of the incident E-field and approximately $\lambda_0/2$ periodicity along the other in-plane direction. In addition, classical metallic lenses display Fresnel reflection losses given the mismatch between the normalized characteristic line impedance of free space and the waveguides. However, as we have shown here, ENZ lens based on near cut-off waveguides can be designed to be approximately impedance-matched. On the other hand, it exists other kind of

metallic lenses based on stacked subwavelength hole arrays, called extraordinary transmission lenses [34,36], that potentially solve this impedance matching as well. Nevertheless, they achieve it by manipulating the effective permeability of the metamaterial through electrically-coupled cut-off artificial waveguides such that $\epsilon = \mu$ ($-\infty < \epsilon < +\infty$, $-\infty < \mu < +\infty$). In terms of electromagnetic modes, these metamaterial lenses support a mixture of TEM and cut-off TE₂₀ or TM₀₂ (depending on the unit cell dimensions) modes, whereas the lens proposed here supports only a TE₀₁.

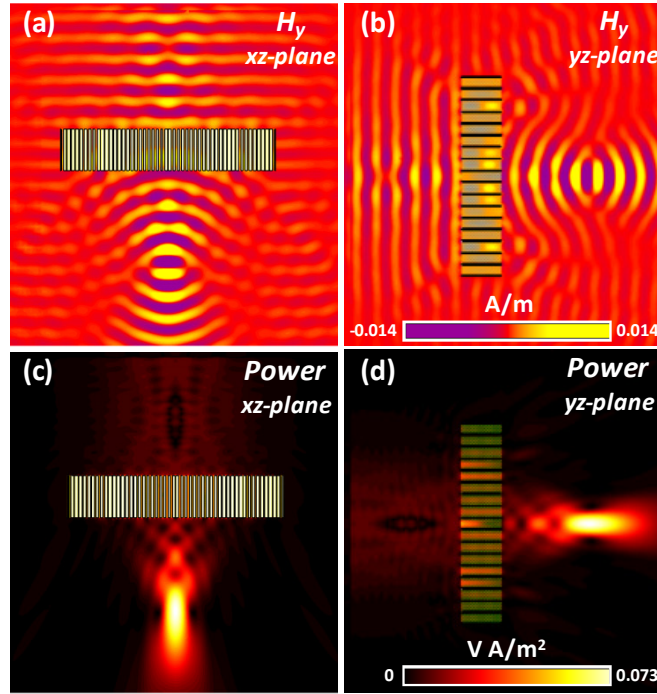


Fig. 6. (a) Top view (xz -plane) and (b) side view (yz -plane) of the magnetic field distribution H_y on a system composed of a three dimensional ENZ lens illuminated by a Gaussian beam. (c) xz -plane and (d) yz -plane of the power distribution on the same system. Scale on panel (b) and (d) is also valid in (a) and (c) respectively.

5. Conclusions

In this article, an arrangement of metallic ENZ waveguides is proposed as a method for planar graded-index lenses. Applying the standard theory of waveguides we are able to match the structure to free-space and individually control the propagation constant inside each waveguide comprising the ENZ metamaterial, tailoring the radiation phase pattern at the exit of the structure to emulate a flat graded-index converging lens. A two-dimensional design of this flat lens working at 1 THz and assuming perfect electrical conductor material is shown, obtaining a good match to the free-space with a reflection coefficient equal to 0.3 and where the importance of the number of waveguides is studied, resulting in a minimum width around $6\lambda_0$ to obtain an acceptable performance. In addition, the chromatic dispersion is studied showing a narrow bandwidth of operation equal to 0.27 THz (26.9% fractional bandwidth). Also a full three-dimensional prototype made of aluminum, in order to consider losses as well, is simulated obtaining a clear focus spot with an enhancement factor of 62.3, a FWHM equal to $1.23\lambda_0/2$ and a depth of focus of $2.05\lambda_0$. This technique may be applied to develop devices that require precise phase control, with low losses, good robustness and small size.

Acknowledgments

In memoriam Prof. Mario Sorolla.

Effort sponsored by Spanish Government under contracts Consolider “Engineering Metamaterials” CSD2008-00066 and TEC2011-28664-C02-01. P.R.-U. is sponsored by the Government of Navarra under funding program “Formación de tecnólogos” 055/01/11. M.N.-C. is supported by the Imperial College Junior Research Fellowship. M. B. acknowledges funding by the Spanish Government under the research contract program Ramon y Cajal RYC-2011-08221. N.E. acknowledges the support from the US Office of Naval Research (ONR) Multidisciplinary University Research Initiatives (MURI) grant number N00014-10-1-0942.